Title

Negative electronic compressibility and tunable spin splitting in WSe2

Journal

Nature Nanotechnology, 10(12)

ISSN

1748-3387

Authors

Riley, JM

Meevasana, W

Bawden, L

et al.

Publication Date

2015-12-01

DOI

10.1038/nnano.2015.217

Peer reviewed

Persistent negative electronic compressibility and tuneable spin splitting in WSe_2

J. M. Riley,[1,2] W. Meevasana,[3,4] L. Bawden,[1] M. Asakawa,[5]
T. Takayama,[6,7] T. Eknapakul,[3] T. K. Kim,[2] M. Hoesch,[2] S.-K. Mo,[8]
H. Takagi,[6,7] T. Sasagawa,[5] M. S. Bahramy,[9,10] and P. D. C. King[1,*]

[1]*SUPA, School of Physics and Astronomy, University of St. Andrews, St. Andrews, Fife KY16 9SS, United Kingdom*

[2]*Diamond Light Source, Harwell Campus, Didcot, OX11 0DE, United Kingdom*

[3]*School of Physics, Suranaree University of Technology, Nakhon Ratchasima, 30000, Thailand*

[4]*NANOTEC-SUT Center of Excellence on Advanced Functional Nanomaterials, Suranaree University of Technology, Nakhon Ratchasima 30000, Thailand*

[5]*Materials and Structures Laboratory, Tokyo Institute of Technology, Kanagawa 226-8503, Japan*

[6]*Department of Physics, University of Tokyo, Hongo, Tokyo 113-0033*

[7]*Max Planck Institute for Solid State Research, 70569 Stuttgart, Germany*

[8]*Advanced Light Source, Lawrence Berkeley National Laboratory, Berkeley, CA 94720, USA*

[9]*Quantum-Phase Electronics Center and Department of Applied Physics, The University of Tokyo, Tokyo 113-8656, Japan*

[10]*RIKEN center for Emergent Matter Science (CEMS), Wako 351-0198, Japan*

(Dated: April 20, 2015)

Tuneable band gaps,[1] extraordinarily large exciton binding energies,[2,3] strong light-matter coupling,[4] and a locking of the electron spin with layer and valley pseudospins[5–9] have established transition-metal dichalcogenides (TMDs) as a unique class of 2D semiconductors with wide-ranging practical applications.[10,11] Using angle-resolved photoemission, we show here that doping electrons at the surface of the prototypical strong spin-orbit TMD WSe_2, akin to applying a gate voltage in a transistor-type device, induces a counterintuitive lowering of the surface chemical potential concomitant with the formation of a multi-valley two-dimensional electron gas (2DEG). These measurements provide a direct spectroscopic signature of negative electronic compressibility, a striking result of electron-electron interactions, which we find persists to carrier densities approximately three orders of magnitude higher than in typical semiconductor 2DEGs that exhibit this effect.[12,13] An accompanying tuneable spin splitting of the valence bands further reveals a complex interplay between single-particle band structure evolution and many-body interactions in electrostatically-doped TMDs. Understanding and exploiting this will open new opportunities for advanced electronic and quantum-logic devices.

Semiconductors are typically considered weakly interacting systems, well described by conventional band theory. In low-dimensional structures, however, the exchange and correlation energies arising from electron-electron interactions can dominate the kinetic energy in the dilute doping limit. This stabilises a small regime of negative electronic compressibility (NEC), $\kappa = \frac{1}{N^2}\frac{\partial N}{\partial \mu} < 0$, whereby increasing the electron density N leads to a decrease of the chemical potential, μ.[12–17] This can drive the system to exhibit exotic correlated states including an enhanced quantum capacitance[14,15,17] and a proposed spontaneous breaking of valley degeneracy.[18]

While of fundamental interest in their own right, such effects are also critical to understanding the evolution of a semiconductor's electronic properties with application of electrical gate voltages - the standard method for field-effect control of semiconductor devices. TMD field-effect transistors have already been fabricated,[11,19] and a range of attractive and intriguing properties uncovered, including chiral light-emission,[20] weak anti-localisation[21] and a density-tuned dome of superconductivity.[22] A detailed understanding of the underlying gate-induced electronic structure evolution driving such emergent properties has, however,

remained elusive.

Here, we mimic the effects of field-effect doping in the TMD WSe_2 by the sub-monolayer deposition of alkali metals at the vacuum-cleaved surface. Such "chemical gating" leaves the surface accessible for detailed spectroscopic measurements. From angle-resolved photoemission (ARPES), we uncover how the resulting charge accumulation drives a pronounced reconstruction of the bulk electronic structure, not only mediating the formation of a multi-valley 2DEG and a giant tuneable valence band spin splitting, but also inducing a pronounced decrease of the surface chemical potential with increasing electron doping. This direct spectroscopic observation of NEC, which we find persists to remarkably high electron densities, reveals a dominant role of many-body interactions shaping the underlying electronic landscape of electrostatically-tuned TMDs.

In Figure 1, we show the occupied electronic structure of bulk and chemically-gated WSe_2 as measured by ARPES. No electronic states cross the Fermi level for the pristine cleaved material (Fig. 1(b)), consistent with its semiconducting bulk. While the uppermost valence bands near the zone centre are strongly three-dimensional, those at the zone-corner $\overline{K}$ point have negligible dispersion along k_z, with electronic wavefunctions localised to single Se-W-Se monlayers (half of the unit cell).[9,23] These two-dimensional states, which form the lowest energy band extrema in monolayer TMDs, are strongly spin-polarised even in the bulk.[6,9] The spin is coupled to the valley degree of freedom, alternating sign at neighbouring corners of the Brillouin zone just as for monolayer MoS_2 and WSe_2.[5,24–26] For the 2H structure, spin also becomes locked to the layer pseudospin, reversing sign for neighbouring Se-W-Se layers.[6,7,9] An energetic degeneracy of the states in neighbouring layers thus enforces the total electronic structure to be spin degenerate, as required by the structural inversion symmetry of bulk WSe_2 (Fig. 1(a)).

We show that breaking such inversion symmetry, achieved here by our surface doping approach, drives a number of striking changes of the electronic structure (Fig. 1(c)). Deposition of minute quantities of alkali metals, electron doping the surface, causes the conduction band states to become populated at the $\overline{K}$ point (only weakly visible) and approximately mid-way along the $\overline{\Gamma}-\overline{K}$ direction (denoted here as $\overline{T}$). The latter have the larger occupied bandwidth, maintaining an indirect band gap as for bulk WSe_2. Unlike in the bulk, however, the conduction bands we observe at $\overline{T}$ have negligible dispersion along k_z, as revealed by our photon energy-dependent measurements (Supplementary Fig. S1). We attribute this

reduced dimensionality as a result of quantum confinement in the surface quantum well created by chemical gating.[27,28] As the band extrema are located away from the zone centre in WSe_2, here this drives the formation of a multi-valley 2DEG (Fig. 1(d)).

The corresponding electrostatic potential variation also lifts the layer degeneracy along z. Our ARPES measurements reveal how this induces a splitting of the layer-localised bulk valence band states at $\overline{K}$ (Fig. 1(e)). Four distinct bands are visible within our probing depth (~ 2 Se-W-Se units[29]) following chemical gating. From their relative intensity variations and energy separations, we can unambiguously assign the "L1" states in Fig. 1(e) as being derived from the first Se-W-Se layer in real space, with the "L2" states localised on layer 2. Due to the intrinsic spin-valley-layer locking of this compound,[6,9] such energetic splittings directly translate to a spin splitting in momentum space (Fig. 1(a)). Our measurements as a function of surface electron doping (Fig. 2) reveal how this effect is broadly tuneable. We find a monotonic enhancement of spin splitting with increasing 2DEG density, reaching values of more than 180 meV for $N \sim 9 \times 10^{13}$ cm^{-2}. This supports recent theoretical suggestions that a field-tuned spin splitting drives the emergence of weak anti-localisation in electric-double-layer WSe_2 transistors.[21] Moreover, the splittings observed here, being directly tied to the electrostatic potential difference between neighbouring layers, reach two orders of magnitude larger than can typically be achieved through gate-voltage control in conventional strong spin-orbit semiconductors,[30] opening new prospects for room-temperature spintronic devices.

The surface electron doping which drives this would conventionally be assumed to increase the binding energy of the valence band states near the surface (Fig. 3(a)). Surprisingly, however, we find an anomalous shift of the valence bands to *lower* binding energy with increasing electron doping (Fig. 3(b)). Over the range of 2DEG densities spanned by our measurements, a simple band bending calculation[31] implies an increase in binding energy of the valence band states localised on the first W layer, Δ_{L1}, of more than 200 meV. In contrast, we find a decrease in binding energy of $\sim$50 meV for Δ_{L1}, and a decrease of almost 150 meV for Δ_{L2}. A naive interpretation of such shifts in terms of conventional semiconductor space-charge regions would not only imply an unphysical opposite band bending for the conduction and valence bands at the surface, but would also be inconsistent with our experimental identification of "layer 1" and "layer 2" derived valence band states at $\overline{K}$. Rather, we assign this as a spectroscopic observation of a lowering of the chemical potential relative to the

valence band edges in the near-surface region (Fig. 3(c)). The negative shifts of the valence states localised on layer 1 are smaller than those for layer 2 due to the larger contribution of single-particle downward band bending to the former, which would conventionally increase their binding energy in competition to the lowering of the chemical potential. Indeed, the rapid decrease of band bending into the bulk allows us to use the "layer 2" states as a reference level, from which we experimentally extract a lower limit of the chemical potential shift ($\Delta\mu$, Fig. 3(d)), which monotonically decreases with increasing 2DEG density.

This is a direct signature of negative electronic compressibility. Strikingly, we find that $\mathrm{d}\mu/\mathrm{d}N < 0$ up to our highest measured electron densities of almost 10^{14} cm^{-2}. In contrast, NEC in GaAs/AlGaAs 2DEGs is observed only at electron densities almost three orders of magnitude lower,[12] while in graphene NEC is found only once a magnetic field suppresses the kinetic energy.[17] The observation of such a persistent NEC here indicates a powerful role of many-body interactions, whereby exchange and correlation energies dominate the kinetic energy over a remarkably large carrier density range. We attribute this to a combination of factors. The 6-valley $\overline{T}$ 2DEG and relatively high effective mass ensures the kinetic energy stays comparably low even for high electron densities, while together with low dielectric constants these enhance the exchange and correlation energies, allowing them to dominate the kinetic energy for a wider range of carrier densities. This is fully supported by our model calculations of exchange and correlation energies within the random phase approximation (RPA, see methods) which predict a broad regime of NEC in this system (Fig. 3(d)). In particular, including the effects of a finite thickness of the 2DEG,[32] we find quantitative agreement between the calculated chemical potential decrease with our extracted values of $\Delta\mu_{exp}$ over an extended carrier density range. This is in strong support of our findings of NEC up to extremely high carrier densities in WSe_2 2DEGs.

We also note that transport signatures of NEC have recently been observed in electrically-gated MoS_2,[33] albeit at lower carrier densities, suggesting that these effects are a general feature of electrostatically-tuned transition-metal dichalcogenides. They can therefore be expected to have a dominating effect in transistor-style applications based on these compounds. Moreover, NEC leads to a negative quantum capacitance which adds in series with the conventional geometrical capacitance. In $SrTiO_3$-based 2DEGs, this has recently been shown to lead to a 40% capacitance enhancement.[15] Similar effects may be a driving force of the known high capacitance of transition-metal dichalcogenides, underpinning their use

as supercapacitors.[34]

Unlike in the case of bulk doping,[35] however, here the emergence of NEC is intricately linked to single-particle band structure changes as a consequence of electrostatic band bending potentials and resultant quantum size effects. To disentangle these, we show in Fig. 4 model surface-projected electronic structure supercell calculations. For the pristine bulk material (Fig. 4(a)), our calculations reproduce the two 2D valence bands at $\overline{K}$ observed experimentally (Fig. 1(b)). The strong spin-polarisation evident in calculations of these states reflects the intrinsic spin-layer locking in this system discussed above. Finite net spin-polarisation results due to the exponential suppression of spectral weight with layer depth employed in our model to reflect the situation for photoemission spectra, and is indeed observed experimentally using this surface-sensitive probe.[9] Our calculations incorporating a downward band bending confirm how these valence bands split into a ladder of strongly spin-polarised states (Fig. 4(b)). Additionally including exchange and correlation effects in our calculation (Fig. 4(c)) maintains this ladder of spin-polarised states, but shifts these to lower binding energy, consistent with our experimental observations.

Together, these reveal how both single-particle band bending and many-body effects collectively drive a rich reconstruction of the near-surface electronic structure of WSe_2. It is evident from Figs. 4(b,c) how this also mediates a pronounced reduction of the quasiparticle band gap, the most fundamental property of a semiconductor, close to its surface. This is supported by our experiment, where we can directly extract indirect band gaps from our ARPES measurements (Fig. 4(d)). These reveal a large layer-dependent band gap reduction, reaching ~ 100 meV even for the first layer where, as evident in Fig. 4(b), quantum size effects naturally increase the surface band gap in the absence of NEC.

A similar doping-induced band gap shrinkage has recently been predicted for monolayer MoS_2.[36] It can also be inferred from previous measurements of monolayer $MoSe_2$, where a band gap of less than 1.6 eV has been observed in heavily electron doped samples,[29] significantly smaller than the single-particle gap in undoped samples.[2] We thus expect our findings of large and persistent NEC to also hold for monolayer TMDs. Together with the observation of extraordinarily strong exciton and trion binding energies in such materials,[2,3,37] our findings establish transition-metal dichalcogenides as strongly interacting systems, opening new potential for controlling, and ultimately exploiting, their optoelectronic and spintronic properties for a new generation of multifunctional electronic devices.

Methods

ARPES: ARPES measurements were performed at the I05 beamline of Diamond Light Source (DLS), UK, and beamline 10.0.1 at the Advanced Light Source (ALS), USA. Single-crystal samples of WSe_2, grown by the chemical vapour transport method, were cleaved *in-situ* and measured at temperatures below 30 K. Measurements were performed using p-polarised synchrotron light from 20 to 150 eV, and employing Scienta R4000 hemispherical electron analysers. Surface electron doping was achieved by evaporating either potassium or rubidium from a properly outgassed SAES getter source onto the sample surface at the measurement temperature. The resulting 2DEG density was determined from the Luttinger area of the Fermi surface at $\overline{T}$, $N = g_v k_F^2/2\pi$ where $g_v = 6$ is the valley multiplicity.

Calculations: The exchange (exc) and correlation (corr) energies per electron were calculated within the random phase approximation as:[33]

$$E_{exc} = -\frac{16}{3\pi(g_v g_s)^{1/2}}\left(\frac{\mathrm{Ry}^*}{r_s}\right)$$

$$E_{corr} = \frac{4}{g_v^2 g_s^2}\left(\frac{\mathrm{Ry}^*}{\pi r_s^2}\right)\int q\mathrm{d}q \int \mathrm{d}w\left(r_s\frac{(g_v g_s)^{3/2}}{2q}\chi(q,\mathrm{i}w) + \ln\left(1 - r_s\frac{(g_v g_s)^{3/2}}{2q}\chi(q,\mathrm{i}w)\right)\right)$$

where $g_v = 6$ and $g_s = 2$ are the valley- and spin-degeneracy, $\mathrm{Ry}^* = \mathrm{Ry}\ m^*/\epsilon_{tot}^2$ is the reduced Rydberg constant, $r_s = m^*/(\epsilon_{tot} a_B(\pi N)^{1/2})$ is the dimensionless interparticle separation parameter, a_B is the Bohr radius and $\chi(q,\mathrm{i}w)$ is the 2D Lindhard function for the dimensionless wave vector along the imaginary axis. We use a 2DEG effective mass of $m^* = 0.555\ \mathrm{m}_e$ and an in-plane and out-of-plane WSe_2 dielectric constant of $\epsilon^{\parallel}_{WSe_2} = 4.2$ and $\epsilon^{\perp}_{WSe_2} = 12.7$, respectively. For the ideal 2DEG calculation, we average these with the vacuum dielectric constant to take account of penetration of the field lines into vacuum. For the finite-thickness calculation, we introduce a form factor $f(q)$ with $\epsilon_{tot}(q) = \epsilon_{WSe_2}/f(q)$. Assuming a triangular potential well,[38] the form factor is given by

$$f(q) = \frac{8 + 9x + 3x^2}{8(1+x)^3} + \frac{\epsilon_{WSe_2} - \epsilon_{vac}}{\epsilon_{WSe_2} + \epsilon_{vac}}\frac{1}{(1+x)^6}, \quad (1)$$

where $x = q/b$ and we take $b = 3\ \text{Å}^{-1}$ to give a 2DEG localised over approximately 5 Å.

A DFT calculation was performed for bulk WSe_2 using the Perdew-Burke-Ernzerhof exchange-correlation potential modified by the Becke-Johnson potential as implemented in the WIEN2K

programme.[41] Relativistic effects, including the spin-orbit interaction, were fully taken into account. The Brillouin zone was sampled by a $12 \times 12 \times 6$ k-mesh. The tight-binding supercell calculations were performed by downfolding these calculations using maximally localised Wannier functions,[39] employing W $5d$ and $5s$ and Se $5p$ and $5s$ orbitals as basis states. Band bending was additionally included as an on-site potential term.[28,40] The single-particle band bending potential was calculated within a solution of Poisson's equation within a modified Thomas-Fermi formalism[31] with an additional potential contribution for the conduction bands due to many-body exchange and correlation effects incorporated from our RPA calculations. The chemical potential was renormalised to maintain the same layer-dependent charge density as for the non-interacting system. To account for the surface sensitivity of AREPS measurements, the spectral weight calculated for each WSe_2 layer was multiplied by an exponential decay function e^{-z/λ_e}, where z is the distance from the surface and λ_e is the inelastic mean free path of the photo-electrons. Here, we assume $\lambda_e = 5$ Å.

Acknowledgements

This work was supported by the Engineering and Physical Sciences Research Council, UK, TRF-SUT Grant RSA5680052 and NANOTEC, Thailand through the CoE Network. PDCK acknowledges support from the Royal Society through a University Research Fellowship. MSB was supported by the Grant-in-Aid for Scientific Research (S) (No. 24224009) from the Ministry of Education, Culture, Sports, Science and Technology (MEXT) of Japan. The Advanced Light Source is supported by the Director, Office of Science, Office of Basic Energy Sciences, of the U.S. Department of Energy under Contract No. DE-AC02-05CH11231. We thank Diamond Light Source for access to beamline I05 (proposal numbers SI9500 and SI11383) that contributed to the results presented here.

---

* To whom correspondence should be addressed: philip.king@st-andrews.ac.uk

[1] Mak, K. F., Lee, C., Hone, J., Shan, J. & Heinz, T. F. Atomically thin MoS_2: A new direct-gap semiconductor. *Phys. Rev. Lett.* **105** (2010).

[2] Ugeda, M. M. *et al.* Giant bandgap renormalization and excitonic effects in a monolayer transition metal dichalcogenide semiconductor. *Nature Mat.* **13** 1091-1095 (2014).

[3] Ye, Z. *et al.* Probing excitonic dark states in single-layer tungsten disulphide. *Nature* **513**,

214–218 (2014).

[4] Liu, X. *et al.* Strong light-matter coupling in two-dimensional atomic crystals. *Nature Photon.* **9**, 30–34 (2015).

[5] Xiao, D., Liu, G.-B., Feng, W., Xu, X. & Yao, W. Coupled spin and valley physics in monolayers of MoS_2 and other group-VI dichalcogenides. *Phys. Rev. Lett.* **108**, 196802 (2012).

[6] Gong, Z. *et al.* Magnetoelectric effects and valley-controlled spin quantum gates in transition metal dichalcogenide bilayers. *Nature Commun.* **4**, 2053 (2013).

[7] Xu, X., Yao, W., Xiao, D. & Heinz, T. F. Spin and pseudospins in layered transition metal dichalcogenides. *Nature Phys.* **10**, 343–350 (2014).

[8] Mak, K. F., McGill, K. L., Park, J. & McEuen, P. L. The valley Hall effect in MoS_2 transistors. *Science* **344**, 1489–1492 (2014).

[9] Riley, J. M. *et al.* Direct observation of spin-polarized bulk bands in an inversion-symmetric semiconductor. *Nature Phys.* **10**, 835–839 (2014).

[10] Wang, Q. H., Kalantar-Zadeh, K., Kis, A., Coleman, J. N. & Strano, M. S. Electronics and optoelectronics of two-dimensional transition metal dichalcogenides. *Nature Nano.* **7**, 699–712 (2012).

[11] Zhang, Y., Ye, J., Matsuhashi, Y. & Iwasa, Y. Ambipolar MoS_2 thin flake transistors. *Nano Letters* **12**, 1136–1140 (2012).

[12] Eisenstein, J., Pfeiffer, L. & West, K. Negative compressibility of interacting two-dimensional electron and quasiparticle gases. *Phys. Rev. Lett.* **68**, 674–677 (1992).

[13] Eisenstein, J., Pfeiffer, L. & West, K. Compressibility of the two-dimensional electron gas: Measurements of the zero-field exchange energy and fractional quantum Hall gap. *Phys. Rev. B* **50**, 1760–1778 (1994).

[14] Ilani, S., Donev, L. a. K., Kindermann, M. & McEuen, P. L. Measurement of the quantum capacitance of interacting electrons in carbon nanotubes. *Nature Phys.* **2**, 687–691 (2006).

[15] Li, L. *et al.* Very large capacitance enhancement in a two-dimensional electron system. *Science* **332**, 825–828 (2011).

[16] Tinkl, V., Breitschaft, M., Richter, C. & Mannhart, J. Large negative electronic compressibility of LaAlO-SrTiO interfaces with ultrathin LaAlO layers. *Phys. Rev. B* **86**, 075116 (2012).

[17] Yu, G. L. *et al.* Interaction phenomena in graphene seen through quantum capacitance. *Proceedings of the National Academy of Sciences* **110**, 3282–3286 (2013).

[18] Bloss, W. L., Sham, L. J. & Vinter, V. Interaction-induced transition at low densities in silicon inversion layer. *Phys. Rev. Lett.* **43**, 1529–1532 (1979).

[19] Radisavljevic, B., Radenovic, A., Brivio, J., Giacometti, V. & Kis, A. Single-layer MoS_2 transistors. *Nature Nano.* **6**, 147–150 (2011).

[20] Zhang, Y. J., Oka, T., Suzuki, R., Ye, J. T. & Iwasa, Y. Electrically switchable chiral light-emitting transistor. *Science* **344**, 725–728 (2014).

[21] Yuan, H. *et al.* Zeeman-type spin splitting controlled by an electric field. *Nature Phys.* **9**, 563–569 (2013).

[22] Ye, J. T. *et al.* Superconducting dome in a gate-tuned band insulator. *Science* **338**, 1193–1196 (2012).

[23] Finteis, T. *et al.* Occupied and unoccupied electronic band structure of WSe2. *Phys. Rev. B* **55**, 10400–10411 (1997).

[24] Mak, K. F., He, K., Shan, J. & Heinz, T. F. Control of valley polarization in monolayer MoS_2 by optical helicity. *Nature Nano.* **7**, 494–498 (2012).

[25] Zeng, H., Dai, J., Yao, W., Xiao, D. & Cui, X. Valley polarization in MoS_2 monolayers by optical pumping. *Nature Nano.* **7**, 490–493 (2012).

[26] Jones, A. M. *et al.* Optical generation of excitonic valley coherence in monolayer WSe_2. *Nature Nano.* **8**, 634–638 (2013).

[27] King, P. D. C. *et al.* Large tunable Rashba spin splitting of a two-dimensional electron gas in Bi_2Se_3. *Phys. Rev. Lett.* **107**, 096802 (2011).

[28] Bahramy, M. *et al.* Emergent quantum confinement at topological insulator surfaces. *Nature Commun.* **3**, 1159 (2012).

[29] Zhang, Y. *et al.* Direct observation of the transition from indirect to direct bandgap in atomically thin epitaxial $MoSe_2$. *Nature Nano.* **9**, 111–115 (2014).

[30] Nitta, J., Akazaki, T., Takayanagi, H. & Enoki, T. Gate control of spin-orbit interaction in an inverted $In_{0.53}Ga_{0.47}As/In_{0.52}Al_{0.48}As$ heterostructure. *Phys. Rev. Lett.* **78**, 1335–1338 (1997).

[31] King, P. D. C., Veal, T. D. & McConville, C. F. Nonparabolic coupled Poisson-Schrödinger solutions for quantized electron accumulation layers: Band bending, charge profile, and subbands at InN surfaces. *Phys. Rev. B* **77**, 125305 (2008).

[32] Das Sarma, S., Jalabert, R. & Yang, S.-R. E. Band-gap renormalization in semiconductor quantum wells. *Phys. Rev. B* **41**, 8288–8294 (1990).

[33] Larentis, S. *et al.* Band offset and negative compressibility in graphene-MoS_2 heterostructures. *Nano. Letters* **14**, 2039–2045 (2014).

[34] Cao, L. *et al.* Direct laser-patterned micro-supercapacitors from paintable MoS_2 films. *Small* **9**, 2905–2910 (2013).

[35] He, J. *et al.* Spectroscopic evidence for negative electronic compressibility in a quasi-three-dimensional spin-orbit correlated metal. *arXiv:1409.8253 [cond-mat]* (2014).

[36] Liang, Y. & Yang, L. Carrier plasmon induced nonlinear band gap renormalization in two-dimensional semiconductors. *Phys. Rev. Lett.* **114** 063001 (2014).

[37] Mak, K. F. *et al.* Tightly bound trions in monolayer MoS_2. *Nature Mat.* **12**, 207–211 (2013).

[38] Vinter, B. Many-body effects in n-type Si inversion layers. I. Effects in the lowest subband. *Phys. Rev. B* **13**, 4447–4456 (1976).

[39] Souza, I. *et al.* Maximally Localized Wannier Functions for Entangled Energy Bands. *Phys. Rev. B* **65**, 035109 (2001).

[40] King, P. D. C. *et al.* Quasiparticle dynamics and spin-orbital texture of the $SrTiO_3$ two-dimensional electron gas. *Nature Commun.* **5**, 3414 (2014).

[41] Blaha, P. et al., WIEN2K package, Version 10.1 (2010); available at, http://www.wien2k.at.

Figure Captions:

FIG. 1: **Electronic structure evolution of chemically-gated WSe_2.** (a) Crystal structure of WSe_2, consisting of Se-W-Se monolayers stacked along the c-axis, with successive layers rotated in-plane by 180°. Electronic states localised to individual layers (e.g. valence bands around $\overline{K}$) are strongly spin-polarised with the spin locked to a layer psuedospin, alternating sign between neighbouring layers, maintaining overall spin degeneracy as shown schematically (upper panel).[6,9] Surface electron doping (lower panel) breaks the layer (and therefore spin) degeneracy. ARPES measurements of (b) bulk-cleaved (hν=75eV) and (c) surface Rb-dosed (hν=49eV) WSe_2. In the latter, electron-like bands intersect the Fermi level giving rise to a multi-valley Fermi surface shown (h$\nu = 75$ eV) in (d). The near-surface electrostatic potential variation that drives this also induces a strong spin-splitting between layer 1 ("L1") and layer 2 ("L2") localised valence band states at $\overline{K}$, shown magnified in (e).

FIG. 2: **Tuneable valley spin splitting.** (a) ARPES measurements of the dispersion of the 2DEG formed at $\overline{T}$ (measured along the $\overline{\Gamma}-\overline{K}$ direction as shown inset) as a function of increasing surface doping. The associated Fermi surface evolution is shown over $k_{x,y} = k_{\overline{T}} \pm 0.17$ Å^{-1}. (b) Corresponding evolution of the lowest binding energy valence bands at $\overline{K}$, revealing a spin splitting that is markedly enhanced with increasing 2DEG density. (c) Extracted density dependence of the spin splitting, Δ, determined from fitting energy distribution curves at $\overline{K}$ (see inset). Different symbols represent measurements from different samples.

FIG. 3: **Spectroscopic signatures of negative electronic compressibility.** (a) Conventional picture of semiconductor charge accumulation layers driven by surface electron doping. A quantum well state (QWS) is formed in the downward band bending potential of the conduction band, while the binding energy of valence states in near-surface layers (Δ_{L1}, Δ_{L2}) grow with increasing surface electron density. (b) In contrast, measurements of Δ_{L1} and Δ_{L2}, determined from fitting energy distribution curves of the uppermost valence band states at $\overline{K}$, reveal a pronounced decrease in binding energy with increasing surface electron density. This is a direct spectroscopic signature of negative electronic compressibility, whereby a dominance of exchange and correlation over kinetic energies cause a decrease in the chemical potential close to the surface, where the 2DEG is localised. This is represented schematically in (c). Approximating the change in chemical potential, $\Delta\mu$, as the relative doping-dependent shift of Δ_{L2}, we extract a direct experimental measure of the NEC (d). This is in good qualitative (quantitative) agreement with our RPA calculations [orange lines] when neglecting (including) the finite thickness of the 2DEG in our calculations. To allow direct comparison, the calculation and experimental data are aligned for our lowest carrier density measurement.

FIG. 4: **Interplay of band bending and negative compressibility.** Surface-projected tight-binding supercell calculations (see methods) of the electronic structure (top) and spin-projection of the valence bands at $\overline{K}$ (bottom) of (a) pristine bulk WSe_2 and (b) chemically-gated WSe_2 including band bending but no effects of electron interactions, revealing the creation of a 2DEG and spin splitting of the valence bands. (c) Additionally including an exchange and correlation potential derived from our finite-thickness RPA calculations leads to an upward shift of the near-surface valence bands relative to the chemical potential, inducing a shrinkage of the layer-dependent quasiparticle band gap, extracted experimentally in (d).

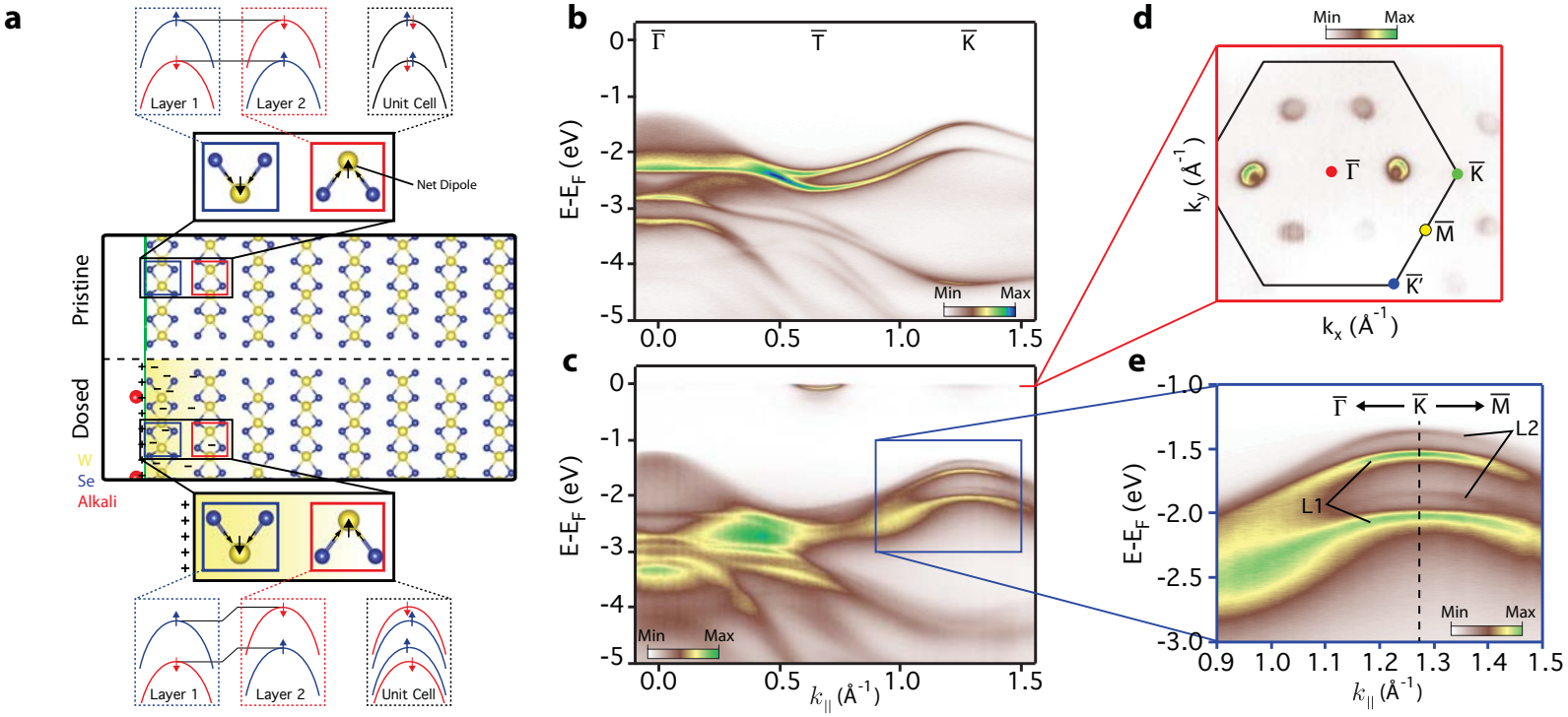
a
Layer 1
Layer 2
Unit Cell
Net Dipole
Pristine
Dosed
W
Se
Alkali
Layer 1
Layer 2
Unit Cell
b
Γ̄
T̄
K̄
E-E_F (eV)
0
-1
-2
-3
-4
-5
Min
Max
0.0
0.5
1.0
1.5
c
E-E_F (eV)
Min
Max
0.0
0.5
k_|| (Å^-1)
1.0
1.5
d
Min
Max
k_y (Å^-1)
Γ̄
K̄
M̄
K̄′
k_x (Å^-1)
e
Γ̄
K̄
M̄
L2
L1
E-E_F (eV)
-1.0
-1.5
-2.0
-2.5
-3.0
Min
Max
0.9
1.0
1.1
1.2
1.3
1.4
1.5
k_|| (Å^-1)

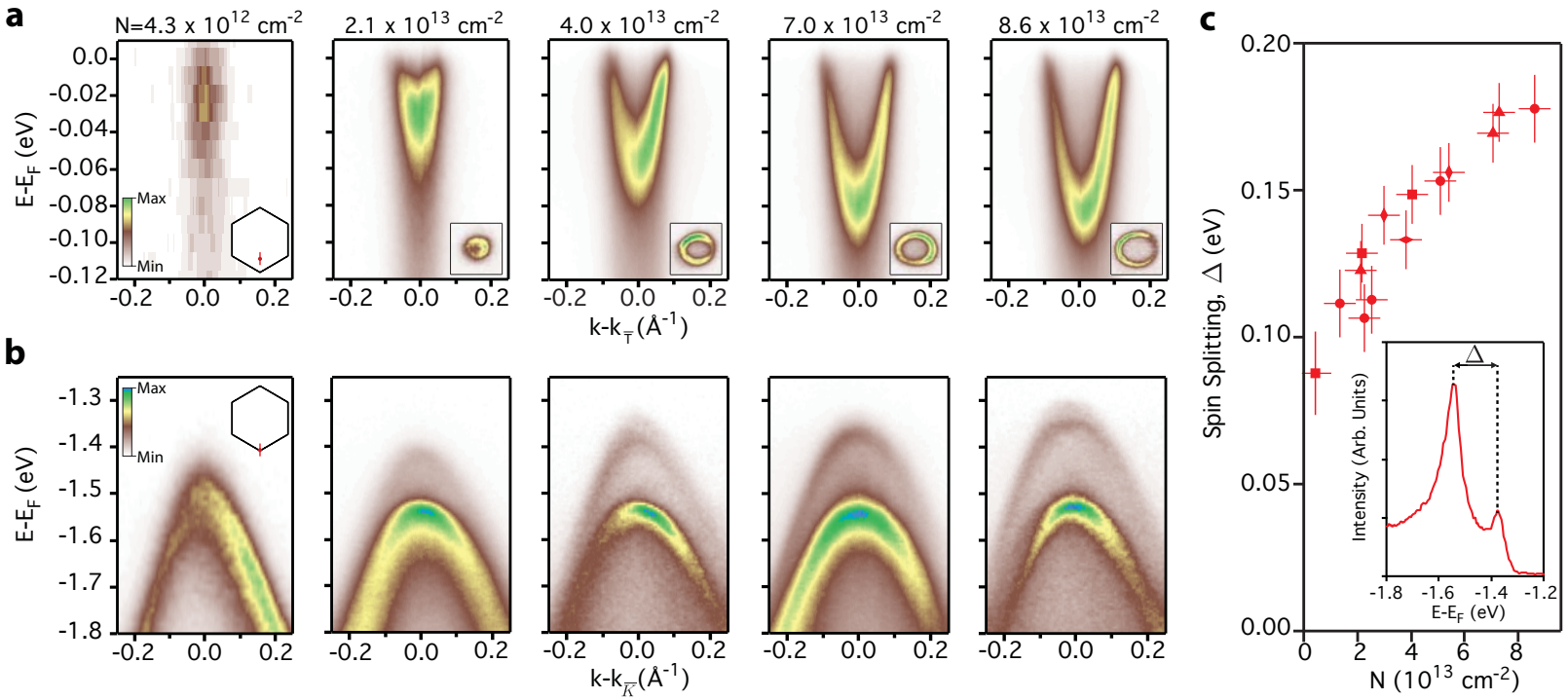
a
N=4.3 x 10^12 cm^-2
2.1 x 10^13 cm^-2
4.0 x 10^13 cm^-2
7.0 x 10^13 cm^-2
8.6 x 10^13 cm^-2
E-E_F (eV)
Max
Min
k-k_Γ̄ (Å^-1)
b
k-k_K̄ (Å^-1)
c
Spin Splitting, Δ (eV)
N (10^13 cm^-2)
Intensity (Arb. Units)
Δ
E-E_F (eV)

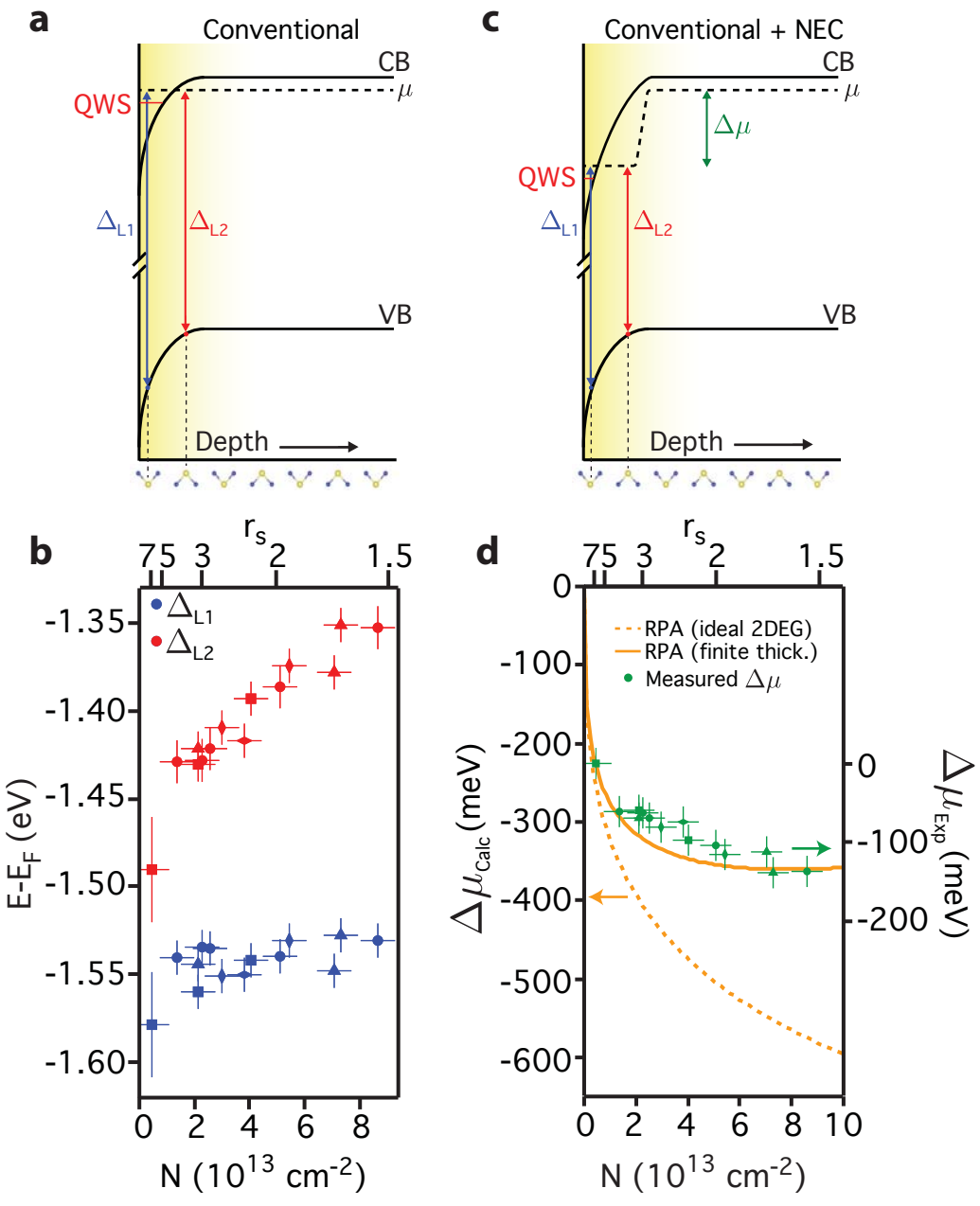
a
Conventional
CB
QWS
μ
Δ_L1
Δ_L2
VB
Depth
c
Conventional + NEC
CB
μ
Δμ
QWS
Δ_L1
Δ_L2
VB
Depth
b
r_s
75 3 2 1.5
Δ_L1
Δ_L2
-1.35
-1.40
-1.45
-1.50
-1.55
-1.60
E-E_F (eV)
0 2 4 6 8
N (10^13 cm^-2)
d
r_s
75 3 2 1.5
RPA (ideal 2DEG)
RPA (finite thick.)
Measured Δμ
0
-100
-200
-300
-400
-500
-600
Δμ_Calc (meV)
0
-100
-200
Δμ_Exp (meV)
0 2 4 6 8 10
N (10^13 cm^-2)

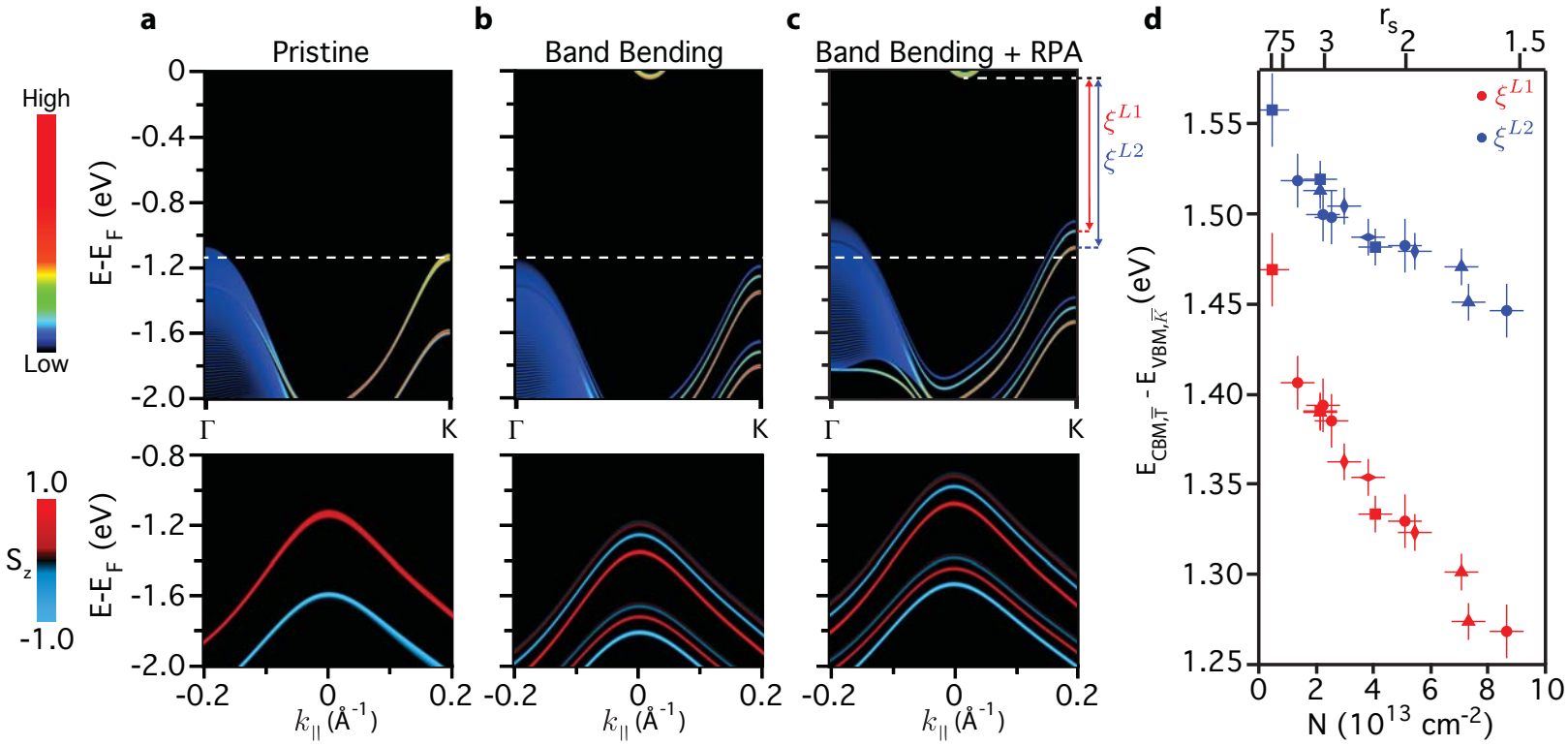
a
Pristine
b
Band Bending
c
Band Bending + RPA
d
High
Low
1.0
S_z
-1.0
E-E_F (eV)
0
-0.4
-0.8
-1.2
-1.6
-2.0
Γ
K
-0.8
-1.2
-1.6
-2.0
-0.2
0
0.2
k_|| (Å^-1)
ξ^L1
ξ^L2
r_s
75
3
2
1.5
E_CBM,Γ̄ - E_VBM,K̄ (eV)
1.55
1.50
1.45
1.40
1.35
1.30
1.25
0
2
4
6
8
10
N (10^13 cm^-2)